Article

Chemistry & Biology

Biochemical Studies of Mycobacterial Fatty Acid Methyltransferase: A Catalyst for the Enzymatic Production of Biodiesel

Graphical Abstract

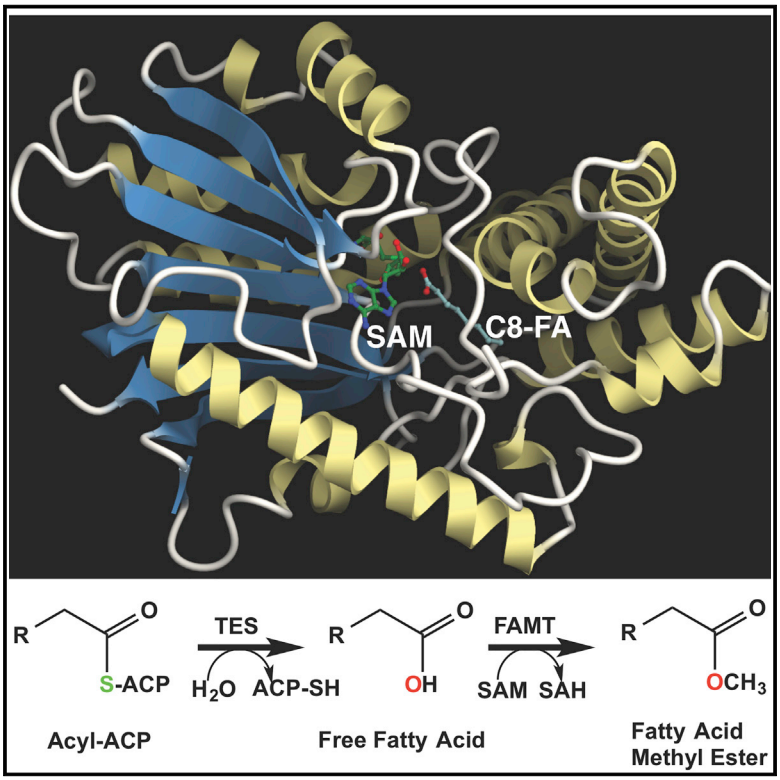

Highlights

- *M. marinum* FAMT catalyzes transesterification of fatty acids to produce biodiesel
- Structure of FAMT reveals similarity to plant primary metabolism methyltransferases
- Kinetic characterization of active-site mutants shows basis for substrate specificity

Authors

Nektaria Petronikolou, Satish K. Nair

Correspondence

snair@illinois.edu

In Brief

Mycobacterial fatty acid methyltransferases are employed as biocatalysts for the production of biodiesel. Petronikolou and Nair describe structural and biochemical characterization of a mycobacterial fatty acid methyltransferase, reveal an unexpected homology to enzymes involved in plant primary metabolism, and provide insights into substrate preference.

Petronikolou & Nair, 2015, Chemistry & Biology *22*, 1–11
November 19, 2015
http://dx.doi.org/10.1016/j.chembiol.2015.09.011

CellPress

Please cite this article in press as: Petronikolou and Nair, Biochemical Studies of Mycobacterial Fatty Acid Methyltransferase: A Catalyst for the Enzymatic Production of Biodiesel, Chemistry & Biology (2015), http://dx.doi.org/10.1016/j.chembiol.2015.09.011

Biochemical Studies of Mycobacterial Fatty Acid Methyltransferase: A Catalyst for the Enzymatic Production of Biodiesel

Nektaria Petronikolou[1,3] and Satish K. Nair[1,2,3,*]
[1]Department of Biochemistry, University of Illinois at Urbana Champaign, 600 South Mathews Avenue, Urbana, IL 61801, USA
[2]Center for Biophysics and Computational Biology and University of Illinois at Urbana Champaign, 600 South Mathews Avenue, Roger Adams Lab Room 430, Urbana, IL 61801, USA
[3]Institute for Genomic Biology, University of Illinois at Urbana Champaign, 600 South Mathews Avenue, Urbana, IL 61801, USA
*Correspondence: snair@illinois.edu
http://dx.doi.org/10.1016/j.chembiol.2015.09.011

SUMMARY

Transesterification of fatty acids yields the essential component of biodiesel, but current processes are cost-prohibitive and generate waste. Recent efforts make use of biocatalysts that are effective in diverting products from primary metabolism to yield fatty acid methyl esters in bacteria. These biotransformations require the fatty acid *O*-methyltransferase (FAMT) from *Mycobacterium marinum* (MmFAMT). Although this activity was first reported in the literature in 1970, the FAMTs have yet to be biochemically characterized. Here, we describe several crystal structures of MmFAMT, which highlight an unexpected structural conservation with methyltransferases that are involved in plant natural product metabolism. The determinants for ligand recognition are analyzed by kinetic analysis of structure-based active-site variants. These studies reveal how an architectural fold employed in plant natural product biosynthesis is used in bacterial fatty acid *O*-methylation.

INTRODUCTION

The increasing demand for energy, coupled with the need for energy independence and security, have been the main forces driving the growing interest in the use of biofuels as a potential sustainable energy resource. The Energy Independence and Security Act of 2007 mandates increased production of biofuels with the aim of reducing the national dependence on unstable foreign suppliers, as well as reducing pollutants produced by the consumption of fossil fuels (US Government, 2007). Although biofuels hold great promise, the current methodologies used for their production require large quantities of water, fertilizers, and pesticides, rendering biofuels less environmentally friendly and sustainable than desired (Naik et al., 2010).

In recent years, biodiesel has emerged as a viable resource for utilization in green energy production. In addition to favorable properties such as biodegradability and low toxicity, biodiesel has properties similar to those of petro-diesel, and can be used as a motor fuel without major engine modifications (Demirbaş, 2002). It is a mixture of long-chain fatty acid alkyl esters (FAAEs), produced mainly by the transesterification of fatty acids derived from vegetable oils and animal fats (Atadashi et al., 2010). Many biodiesel precursors are derived from triglycerides, which are esters of three equivalents of fatty acids with one equivalent of glycerol. Triglycerides can undergo transesterification with an alcohol in the presence of a catalyst to yield FAAEs and glycerol as final products. However, this process is expensive and generates waste, negating the financial and environmental benefits of using biodiesel (Leung et al., 2010).

With the goal of formulating less energy-intensive and more environment-friendly methods for biodiesel production, several laboratories have engineered microorganisms for the overproduction of fatty acid precursors (Kung et al., 2012; Steen et al., 2010; Li et al., 2008; Nawabi et al., 2011). More recently, *Escherichia coli* has been engineered to directly produce fatty acid methyl esters (FAMEs) and 3-hydroxy fatty acid methyl esters (3-OH FAMEs) by using a fatty acid *O*-methyltransferase (FAMT) from *Mycobacterium marinum* (MmFAMT) for transesterification in situ (Figure 1A) (Nawabi et al., 2011). Although the yield of FAMEs produced by this pathway was lower than the maximal FAAE yields reported (Steen et al., 2010; Nawabi et al., 2011), the use of FAMT holds promise for in vivo biodiesel production.

The fatty acid *O*-methyltransferases are *S*-adenosylmethionine (SAM)-dependent enzymes that catalyze the transfer of a methyl group to the carboxyl group of a fatty acid acceptor (Struck et al., 2012). Canonical SAM-dependent methyltransferases catalyze alkylation on heteroatoms via an S_N2-type nucleophilic substitution mechanism (Blumenthal et al., 1999). Mycobacteria specifically possess a large number of SAM-dependent methyltransferases that catalyze the modification of mycolic acids, the very long fatty acids found in mycobacterial cell walls (Barry et al., 1998). These enzymes can be broadly classified with regard to the identity of the methyl acceptor, and include the cyclopropane fatty acid synthases (which catalyze *C*-methylation of a *cis* double bond) (Huang et al., 2002), and the *O*-methyltransferases that catalyze methylation on the hydroxyl moiety of phthiocerol, phenolphthiocerol, or ketomycolate (Yuan et al., 1998; Yuan and Barry, 1996). There are three cyclopropane fatty acid synthases with different regiospecificities; CmaA1 catalyzes the installation

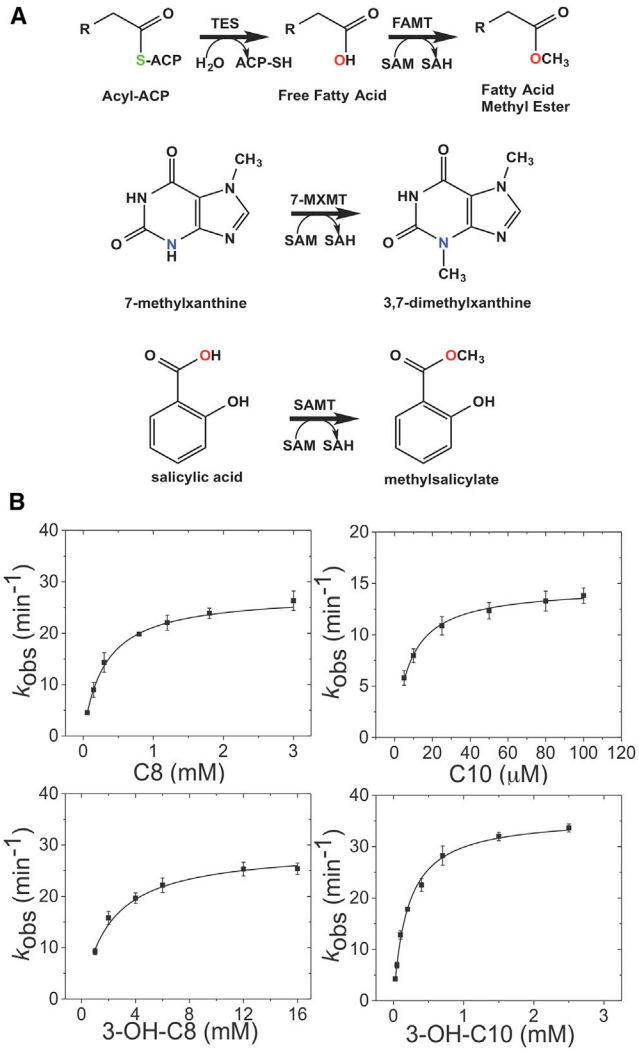

Figure 1. Small Molecule Methyltransferase Reactions and Michaelis-Menten Kinetics

(A) Reactions catalyzed by the fatty acid *O*-methyltransferase (FAMT) and two of its structural homologs from the SABATH family (7-MXMT, 7-methylxanthine *N*-methyltransferase; SAMT, salicylic acid *O*-methyltransferase). Free fatty acids can be released by the action of a thioesterase (TES) on acyl-ACP (acyl carrier protein).

(B) Michaelis-Menten kinetic plots for the wild-type MmFAMT for octanoate (C8), decanoate (C10), 3-hydroxyoctanoate (3-OH-C8), and 3-hydroxydecanoate (3-OH-C10). All measurements were conducted in triplicate and the mean average value for each are shown. Error bars indicate the standard deviations of each data point.

of the distal cyclopropane ring on α-mycolic acid when overexpressed (Yuan et al., 1995; Glickman, 2003), PcaA installs that proximal cyclopropane ring in α-meroacid (Glickman et al., 2000), and CmaA2 catalyzes the *cis*-cyclopropane synthesis in methoxymycolates (Yuan and Barry, 1996). Additional examples include MmaA4 that introduces a methyl branch, together with an adjacent hydroxyl group, during the formation of both keto- and methoxymycolates (Boissier et al., 2006). In contrast to these other SAM-dependent enzymes, little is known about FAMTs (Nawabi et al., 2011; Akamatsu and Law, 1970; Orpiszewski et al., 1991; Safayhi et al., 1991; Sastry et al., 1994). Although they were first discovered in mycobacteria in 1970 (Akamatsu and Law, 1970), there are very few published studies about this class of methyltransferases (Nawabi et al., 2011; Akamatsu and Law, 1970; Safayhi et al., 1991), and their physiological role in mycobacteria has yet to be elucidated.

The identification of the mycobacterial FAMTs was facilitated by the sequence analysis of mycobacterial proteins, and sequence-based structural alignments suggested that they contain a Rossmann-like fold found in class I methyltransferases (Liscombe et al., 2012). The primary sequences of the mycobacterial enzymes also suggest weak, but notable, similarities to plant natural product methyltransferases, such as dimethylxanthine methyltransferase (PDB: 2EFJ) (McCarthy and McCarthy, 2007) and salicylate methyltransferase (PDB: 1M6E) (Zubieta et al., 2003), as well as other members of a recently characterized protein family classified as the SABATH methyltransferase (Pfam03492 [D'Auria et al., 2003]; so named for the first characterized members of this fold class) (Figure 1A). However, these plant enzymes are not known to catalyze methylation of fatty acid substrates, and the sequence identity between the mycobacterial enzymes and the plant *O*-methyltransferases is less than 25%.

To understand the basis for this biotechnologically relevant enzyme, we carried out biochemical and biophysical characterization of the MmFAMT that has been previously utilized for the in vivo production of biodiesel (Nawabi et al., 2011). Cocrystal structures of the enzyme with a variety of bound substrates allow for the identification of features that bestow specificity to fatty acid substrates. Kinetic characterization of active-site variants, as deduced from the structural data, facilitates the assignment of roles for various residues and the proposal for a reaction mechanism consistent with the data. These studies should provide a framework for future engineering experiments aimed at adapting FAMTs for in vivo high-yield production of biodiesel from fatty acid precursors.

RESULTS AND DISCUSSION

Kinetic Characterization of *M. marinum* FAMT

The kinetic parameters for wild-type MmFAMT for a panel of fatty acids and 3-hydroxy fatty acids were determined using a coupled assay (Dorgan et al., 2006; Wooderchak et al., 2008) that monitored SAM turnover. In this assay, *S*-adenosylhomocysteine (SAH), the product of SAM, is hydrolyzed by an SAH nucleosidase (the Pfs SAH nucleosidase has a catalytic efficiency of 11.6×10^6 M^{-1} s^{-1} [Choi-Rhee and Cronan, 2005], which is greater than that of MmFAMT) to *S*-ribosylhomocysteine and adenine. The latter is subsequently deaminated by an adenine deaminase, resulting in a decrease in absorbance at 265 nm ($\Delta\varepsilon \approx 6{,}700$ M^{-1} cm^{-1}), and allowing for continuous monitoring of the reaction (Dorgan et al., 2006). The catalytic efficiency of MmFAMT for free fatty acids was found to increase with chain length (the k_{cat}/K_M value for C8 octanoic acid is 1.49×10^3 M^{-1} s^{-1}, and for C10 decanoic acid is 2.97×10^4 M^{-1} s^{-1}) (Table 1 and Figure 1B). The 3-hydroxy compounds were turned over less efficiently, with k_{cat}/K_M values that are roughly an order of magnitude lower than for the corresponding fatty acid. The kinetic parameters for MmFAMT reported here differ from values determined previously via a discontinuous

Table 1. Steady-State Kinetic Parameters for MmFAMT Wild-Type and Mutants Against Different Substrates

MmFAMT	K_M (μM)	k_{cat} (10^{-2} s^{-1})	k_{cat}/K_M (M^{-1} s^{-1})
Wild-Type			
C8	308 ± 9	46.1 ± 0.5	1,497
C10	8.2 ± 0.5	24.4 ± 0.4	29,756
3-OH-C8	2,039 ± 172	48.8 ± 1.4	239
3-OH-C10	201 ± 8	59.9 ± 1.1	2,975
SAM	25.5 ± 4.0	59.8 ± 3.2	23,450
Q31A			
C8	[a]	[a]	[a]
3-OH-C10	[a]	[a]	[a]
Q154A			
C8	5,238 ± 427	14.7 ± 0.4	28.1
3-OH-C10	1,028 ± 43	4.2 ± 0.0	40.9
W155F			
C8	[a]	[a]	1.37 ± 0.03
3-OH-C10	[a]	[a]	3.05 ± 0.16
Y24F			
SAM	[a]	[a]	824 ± 19

[a]Could not be determined.

assay that employed radiolabeled SAM as a donor (Nawabi et al., 2011). These differences likely arise from variations in the two methods used for characterization. However, in the context of this work, our kinetic data provide an internal standard for analyzing the effects of specific amino acid mutations on the catalytic activity of MmFAMT, as reported below.

Binding Affinity of MmFAMT for SAM and SAH

The product SAH is known to inhibit some SAM-dependent methyltransferases. To characterize whether MmFAMT is similarly subject to product inhibition, we carried out isothermal titration calorimetric (ITC) analysis to measure the binding affinity to SAM and SAH (Table S1 and Figure S1). MmFAMT binds to SAM with a dissociation constant (K_D) of 33.6 μM, while binding of SAH occurs with a K_D two orders of magnitude smaller (0.70 μM). For both ligands, binding is driven largely by the enthalpic component. These data are consistent with the inhibition of MmFAMT by the product SAH. It should be noted that all measurements using SAM as the ligand yielded a number of binding sites of two (n = 2.06 ± 0.01), while measurements with SAH gave a number of sites of one (n = 0.93 ± 0.01). The basis for this discrepancy is not clear, as the structural data do not reveal evidence for multiple binding sites. Nonetheless, it is evident from the binding isotherms that MmFAMT binds tightly to SAH. These results are in agreement with product inhibition observed in several members of this family (Kung et al., 2015; Obianyo and Thompson, 2012; Lee et al., 2005). Hence, both in vivo and in vitro efficacy of enzymatic methylation of free fatty acids using FAMTs may be improved if the reactions are coupled to an SAH nucleosidase to hydrolyze the SAH product.

Crystal Structures of MmFAMT

The unique specificity of bacterial FAMTs for fatty acid substrates cannot be understood in the context of the distantly related plant SABATH family of methyltransferases, which share limited sequence similarities (25% sequence identity), and all of which function on small-molecule natural products (Liscombe et al., 2012). To understand this substrate specificity and scope, we determined several binary and ternary complex structures of MmFAMT in complex with SAH (1.7 Å resolution), SAH and octanoate (1.6 Å resolution), and SAH and 3-hydroxydecanoate (1.9 Å resolution). We also determined the structure of an MmFAMT active-site mutant (Q154A) in complex with SAH and 3-hydroxydecanoate (1.85 Å resolution). Initial crystallographic phases were determined by single-wavelength anomalous diffraction using selenomethionine (SeMet)-labeled protein (SAH and decanoic acid), and phases for subsequent structures were determined by molecular replacement using the resultant model as a search probe. All crystallographic data collection and refinement statistics are provided in Table 2.

The overall structure of MmFAMT consists of a di-domain architecture composed of a Rossmann-like α/β fold that is common among diverse class I methyltransferases, which is further elaborated with an all α-helical domain that caps the SAM-binding site (Figure 2A). The Rossmann-like fold core is formed from discontinuous regions of the polypeptide chain and space residues Ser11 through Asp217, Pro255 through Ala287, and Pro354 through the carboxy terminus. This core consists of a seven-stranded β-sheet core that is sandwiched between sets of helical regions. The helical capping domain is similarly composed of disjointed segments and forms part of the active site, in a fashion similar to that found in plant natural product methyltransferases (McCarthy and McCarthy, 2007; Zubieta et al., 2003; Zhao et al., 2008).

Despite a low conservation in primary sequence, a search of the PDB (Bernstein et al., 1977) using the Dali server (Holm and Rosenstrom, 2010) shows that MmFAMT is structurally homologous to the SABATH class of plant natural product methyltransferases, which themselves are only distantly related to other well-characterized small-molecule methyltransferases (D'Auria et al., 2003). Representative structural homologs include the salicylic acid (SA) *O*-methyltransferase from *Clarkia breweri* (PDB: 1M6E; root-mean-square deviation [RMSD] of 2.5 Å over 330 Cα atoms; 23% sequence identity) (Zubieta et al., 2003), the dimethylxanthine *N*-methyltransferase from *Coffea canephora* (PDB: 2EFJ; RMSD of 3.2 Å over 328 Cα atoms; 22% sequence identity) (McCarthy and McCarthy, 2007), and indole-3-acetic acid *O*-methyltransferase from *Arabidopsis thaliana* (PDB: 3B5I; RMSD of 2.6 Å over 312 Cα atoms; 23% sequence identity) (Zhao et al., 2008) (Figure S2). The unexpected structural similarities between MmFAMT and the plant SABATH *O*-methyltransferases reflect the similar substrate repertoires of these enzymes, specifically that they both catalyze methylation of carboxylic acid on an otherwise hydrophobic substrate. However, the nature of the hydrophobic groups differs as the plant enzymes utilize larger, bulkier scaffolds that are typically aromatic, while the FAMTs function on fatty acids containing a long hydrocarbon acyl chain (Figure 1A).

The plant SABATH methyltransferases described above are all homodimers in solution and the corresponding crystal structures demonstrate a two-fold symmetric arrangement. Likewise, MmFAMT is homodimeric both in solution and in the crystal lattice (Figure S3). In plant *O*-methyltransferases that are not members of

Table 2. Data Collection, Phasing, and Refinement Statistics

	Native	SeMet	C8	3-OH-C10	Q154A-3-OH-C10
Data Collection					
Space group	$P2_1$	$P2_1$	$P2_1$	$P2_1$	$P2_1$
a, *b*, *c* (Å), β (°)	63.1, 66.1, 98.4, 107.5	62.7, 65.7, 97.5, 107.8	63.1, 66.1, 98.1, 107.4	62.8, 65.9, 98.2, 107.1	62.8, 65.6, 98.2, 107.3
Resolution (Å)[a]	50–1.7 (1.73–1.7)	50–1.95 (1.98–1.95)	50–1.6 (1.63–1.6)	50–1.9 (1.93–1.9)	50–1.85 (1.88–1.85)
R_{sym} (%)[b]	5.4 (52.1)	5.5 (58.8)	6.0 (57.3)	6.5 (54.1)	7.0 (81.4)
$I/\sigma(I)$	25.6 (2.6)	15.9 (2.2)	20.5 (1.9)	18.2 (2.1)	14.5 (1.9)
Completeness (%)	100 (99.9)	100 (100)	100 (99.7)	99.5 (100)	100 (100)
Redundancy	5.0 (4.8)	4.1 (4.1)	4.2 (3.5)	4.1 (4.1)	4.7 (4.7)
Phasing					
FOM[c]		0.382/0.157			
Refinement					
Resolution (Å)	25.0–1.7		25.0–1.6	25.0–1.9	25.0–1.85
No. of reflections	80,265		95,148	55,801	61,413
R_{work}/R_{free}[d]	19.5/22.2		19.5/21.8	19.3/23.1	19.3/22.4
No. of atoms					
Protein	5,504		5,533	5,525	5,525
Fatty acid	-		20	26	44
SAH	52		52	52	52
Water	793		802	563	570
B factors					
Protein	16.7		16.9	24.1	23.9
Fatty acid	-		16.2	17.2	22.2
SAH	7.9		8.1	12.8	12.6
Water	27.9		28.4	30.9	31.2
RMSD					
Bond lengths (Å)	0.000		0.005	0.006	0.006
Bond angles (°)	1.07		1.07	1.15	1.11

[a]Highest-resolution shell is shown in parentheses.
[b]$R_{sym} = \Sigma|(I_i - \langle I_i \rangle)|\Sigma I_i$, where I_i is the intensity of the *i*th reflection and $\langle I_i \rangle$ is the mean intensity.
[c]Mean figure of merit (acentric/centric).
[d]*R* factor = $\Sigma(|F_{obs}| - k|F_{calc}|)/\Sigma\,|F_{obs}|$, and R_{free} is the *R* value for a test set of reflections consisting of a random 5% of the diffraction data not used in refinement.

the SABATH class, notably chalcone *O*-methyltransferase and caffeic acid *O*-methyltransferase, the dimeric arrangement is functional, with residues from one monomer contributing to the active site of the other subunit (Zubieta et al., 2001, 2002). Although the SABATH enzymes are also dimeric, oligomerization is not needed for activity. Oligomerization of MmFAMT is similarly likely not functional, as the monomeric entity contains all of the necessary residues involved in catalysis. Likewise, dimerization only buries ~1,314 Å^2 of solvent-accessible surface area (corresponding to 8% of the total surface area of each monomer), which is far less than for the functionally homodimeric enzymes. The dimerization interface of MmFAMT is similar in organization to that of the SA *O*-methyltransferase (Zubieta et al., 2003) and indole-3-acetic acid *O*-methyltransferase (Zhao et al., 2008), both of which also likely function as a monomer.

SAM/SAH and Substrate-Binding Pockets

Similar to other class I methyltransferases, the SAM/SAH binding site is situated in the Rossmann-like fold domain, and the ligand is bound in an extended manner, roughly perpendicular to the plane of the β strands. In the MmFAMT-SAH structure, the pyrimidine ring of SAH adenine is sandwiched between the side chain of Phe134, via a π-stacking interaction on one side and Val99 on the other (Figure 2B). Extensive hydrogen bonding interactions further stabilize the bound SAH, including the interaction between Ser133 and the adenine amine, between Asp98 and both hydroxyls of the ribose, and between Tyr24 and Ser150 and the α-carboxylate of SAH. Additional contacts are mediated through van der Waals interactions with non-polar residues that contribute to form the SAM/SAH binding site. An analogous network of interacting residues stabilizes bound SAM/SAH in structures of the plant natural product *O*-methyltransferases. The extensive set of interactions and the hydrophobicity of the binding site rationalize why uncharged SAH is a strong competitive inhibitor of MmFAMT.

The cocrystal structure of MmFAMT with SAH and octanoate shows that the substrate-binding site is largely localized within the α-helical domain that caps the Rossmann-like fold domain (Figure S2A). This capping domain contains a binding cavity that is sufficiently contoured to accommodate fatty acid

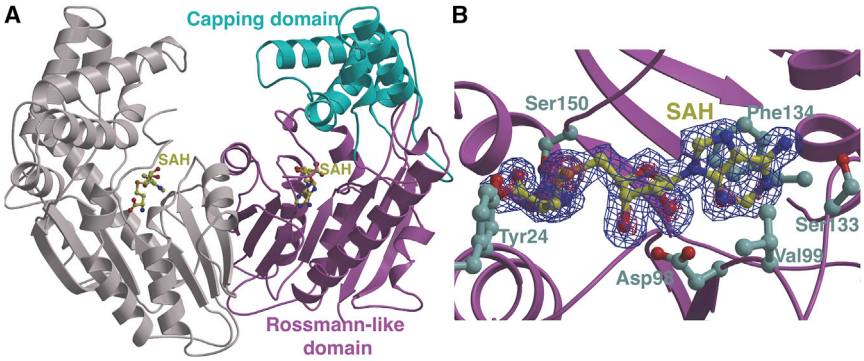

Figure 2. Structure of Fatty Acid Methyltransferase and Binding Pocket of SAM/SAH

(A) Ribbon diagram of the MmFAMT/SAH crystal structure, with one monomer colored in gray and the other colored in purple (Rossmann-like fold domain) and cyan (capping domain).

(B) Simulated annealing difference Fourier map (F_o-F_c) contoured to 2.5σ (blue) and 10σ (red) showing the SAM-binding site of MmFAMT. The coordinates for bound SAH were omitted during map calculations. The bound ligand is colored yellow, and residues that interact with the ligand are colored gray.

substrates with acyl chain lengths up to C12. Numerous aliphatic and aromatic residues encircle the acyl chain of the fatty acid substrate, including Trp155, Met214, Phe222, Tyr224, Val256, Phe311, and Leu316 (Figure 3A). MmFAMT residues Tyr174, Met 227, and Asn228 enclose the upper side of the binding cavity, and multiple conformers are observed for the latter two residues. The planar, extended conformation of the fatty acid substrate is set by the side chains of Met19, Ala315, and Leu316 on one side of the substrate and by Trp151 and Tyr224 on the opposite side. In the SA *O*-methyltransferase cocrystal structure, Met150 and Met308 similarly sandwich the substrate for proper positioning at the SAM methyl donor (Zubieta et al., 2003). Lastly, hydrogen bonding with Gln31 and Trp155 engage and orient the carboxylate moiety of the fatty acid substrate for methyl transfer, similar to the Gln25/Trp151 pair utilized by SA *O*-methyltransferase to orient the carboxylate of its substrate. The relative disposition of the α-helical capping and Rossmann-like fold domains is slightly different than that observed in structures of plant *O*-methyltransferases with a similar bilobed structure, which may also contribute to different substrate scope of the FAMTs (Figure S2).

A comparison of the MmFAMT/SAH cocrystal structures with bound octanoate and 3-hydroxydecanoate suggests a rationale for understanding why MmFAMT shows a preference for the larger substrate (K_M values of C10 substrates lower by a factor of ~10–40 relative to the C8 counterparts; Table 1). While Met227 and Asn228 are observed as multiple conformers in the cocrystal structure with octanoate (Figure 3B), both of these residues exist in single conformations oriented away from the substrate-binding cavity to accommodate the larger acyl chain in the SAH/3-hydroxydecanoate structure (Figure 3D). This movement is accompanied by a compensatory reorganization of a loop spanning residues Leu166 through Gln171, located near the omega carbon of the fatty acid, resulting in tighter packing against C9 and C10 of the acyl chain (Figure 3D). Movement of these side chains fills the substrate-binding cavity but only with acyl chains of length C10–C12, and likely explains why these longer-chain fatty acids are better substrates than octanoate (Figures 3B and 3D). There are limited interactions in the active site with the 3-hydroxyl moiety, as Gln154 is located within hydrogen bonding distance and the thioether of Met214 is more than 3.2 Å away. Placement of the polar 3-hydroxyalcohol in a hydrophobic binding pocket without sufficient compensatory interactions may explain the higher K_M values for 3-hydroxy-containing substrates relative to their acyl counterparts (Table 1). Lastly, Gln154 is positioned to hydrogen bond with the carboxylate of the substrate in the MmFAMT/SAH/octanoate structure. However, a modest rotation of the plane of the substrate, necessary to maximize interactions of the 3-hydroxyl group with Gln154, results in a slight movement of this residue away from the substrate carboxylate in the MmFAMT/SAH/3-hydrodecanoate structure.

In the cocrystal structure of MmFAMT with 3-hydroxydecanoate, only the S enantiomer was bound in the active site, although an enantiomeric mixture of 50% R and 50% S was used in the crystallization condition. This enantiomeric selectivity is due to the presence of hydrophobic residues (Phe311 and Trp151) on one side of the active site in close proximity to the carboxyl group, and the presence of Gln154 on the other side in a position favorable for hydrogen bonding with the 3-hydroxyl group of the S enantiomer. Although the physiological role of MmFAMT is yet to be elucidated, this enantiomeric specificity may be of physiological relevance. 3-Hydroxylated fatty acids are found in mycobacterial phospholipids (Alugupalli et al., 1994, 1995), enter β-oxidation as (S)-3-hydroxyacyl coenzyme A (Shimakata et al., 1979; Williams et al., 2011), and are part of the mycolic acid biosynthesis as (R)-3-hydroxy-acyl-ACP (acyl carrier protein) (Sacco et al., 2007; Marrakchi et al., 2014). Methylation of the carboxyl group of the (S)-3-hydroxy fatty acids may be part of any of these processes by regulating the fate of the (S)-3-hydroxy fatty acids. This hypothesis, however, is yet to be investigated.

Molecular Basis for Fatty Acid Substrate Specificity

As noted, the structure of MmFAMT shares several features with that of SA *O*-methyltransferase (Zubieta et al., 2003), including the presence of a hydrophobic α-helical domain that caps the SAM-binding site. While both enzymes utilize a similar constellation of active-site residues to orient the substrate carboxylate (Gln31/Trp155 in MmFAMT and Gln25/Trp151 in SA *O*-methyltransferase), the capping domain establishes specificity for the hydrophobic part of the substrate (Figures 4A and 4B). Specifically, the contours of each cavity are optimized for its cognate substrate. In SA *O*-methyltransferase the active site is borderlined by Ile 225, Trp226, Tyr255, and Phe347, and in MmFAMT by Tyr174, Phe222, Tyr224, Met227, and Asn228. The replacement of Ile225 and Trp226 (in SA *O*-methyltransferase) by Met227 and Asn228 (in MmFAMT) creates a larger cavity to accommodate the longer acyl chain of the fatty acid (Figures 3, 4A, and 4B).

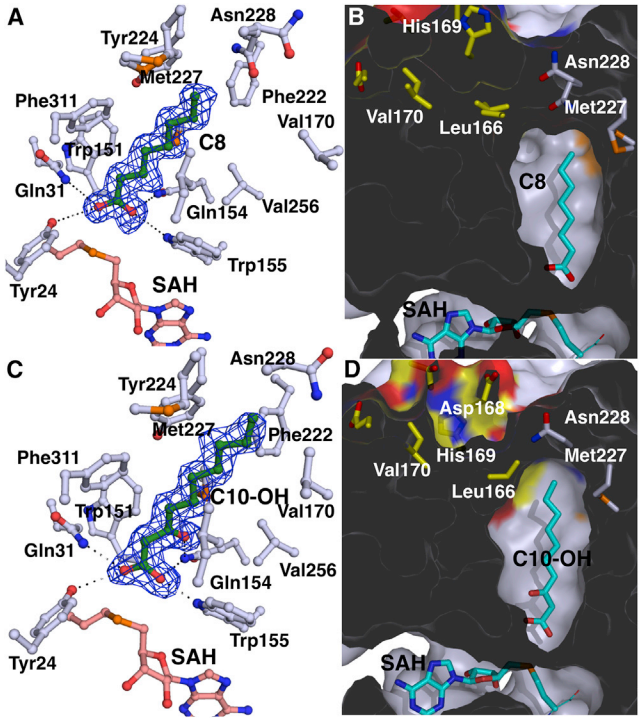

Figure 3. FAMT Active Site with Bound Substrates

(A and C) Difference Fourier maps (F_o-F_c) contoured to 2.5σ (blue) showing the bound fatty acid substrates (colored green).

(B and D) Surface cut-away diagram showing that binding of the larger substrate results in a smaller cavity due to movement of Leu166 through Gln171.

Although the constrained smaller cavity of SA *O*-methyltransferase may not accommodate a fatty acid, the larger cavity of MmFAMT raised the question as to whether MmFAMT can utilize SA as a substrate despite the lack of residues that would anchor the aromatic ring in an optimal orientation. To further investigate this, we carried out reactions (2 hr incubation at 37°C) of MmFAMT with SA in triplicate, and analyzed the products by gas chromatography-mass spectrometry (GC-MS). Surprisingly, MmFAMT is able to catalyze methylation on SA (Table S2). A closer examination of an active-site superposition of the cocrystal structures of MmFAMT/SAH/octanoate and SA *O*-methyltransferase/SAH/SA reveals that SA can be accommodated into the MmFAMT active site. Although the positioning of Phe311 (Cys307 in SA *O*-methyltransferase) would seemingly cause some steric clashes, the residue at the other side of the aromatic ring (Tyr255 in SA *O*-methyltransferase) is a smaller Val256 in MmFAMT, which would allow for positioning of SA as a substrate. Equivalent, but distinct, residues in the MmFAMT active site could orient SA. However, in SA *O*-methyltransferase, Ile225 and Trp226, which are replaced by the aforementioned flexible Met 227-Asn228 in MmFAMT, constrict the upper end of the active site to accommodate the smaller SA substrate (Figures 4A and 4B). Consequently, it is likely that SA may not bind very well in the MmFAMT active site.

Kinetic Analysis of Wild-Type and Mutant MmFAMTs

The cocrystal structures of MmFAMT identified a number of residues that may play a role in either substrate binding or catalysis. To further probe this function, we generated site-specific mutations at several of these residues and determined kinetic parameters for the variant enzymes (Table 1). The Gln31 → Ala mutation had an immense effect on the enzyme activity, as no product formation could be detected even when 20-fold more enzyme and much greater concentrations (up to 5 mM) of substrate were used. Similarly, the Trp155 → Phe mutation resulted in a near 1,000-fold decrease in catalytic efficiency (k_{cat}/K_M). As Gln31 and Trp155 are situated near the carboxylate of the substrate, the Gln31 → Ala and Trp155 → Phe mutations likely compromise binding and orientation of the substrate, consistent with the loss of activity in each of these mutants.

The Gln154 → Ala mutation had a large effect on the K_M of MmFAMT with octanoate as a substrate (17-fold increase), and a smaller effect on the K_M for 3-hydroxydecanoate (5-fold increase). This was an unexpected result, as Gln154 is within hydrogen bonding distance to the 3-hydoxyl group, and a mutation at this residue would be expected to cause a much greater increase in the K_M for the 3-hydroxy fatty acid. To provide a rationale for this observation, we determined the 1.85-Å resolution cocrystal structure of MmFAMT Gln154 → Ala in complex with SAH and 3-hydroxydecanoate. The structure shows that the 3-hydroxyl group rotates toward the sulfur of Met214 to compensate for the loss of interaction with Gln154 (Figure S4), explaining why this mutation results in only a modest increase in the K_M for 3-hydroxydecanoate. The Gln154 → Ala mutation also results in the carboxylate shifting away to result in a less optimal orientation for methyl transfer, consistent with a 10-fold lower k_{cat} for the mutant relative to wild-type MmFAMT.

Conclusions

Our collective structural and biochemical analysis demonstrates how MmFAMT uses a SABATH plant natural product methyltransferase architecture to catalyze the methylation of fatty acid substrates. This adaptation is a result of minor alterations in secondary structural elements, and of the changes in the disposition of the α-helical capping domain, which engages the substrate, relative to the Rossmann-like fold domain that harbors the methyl donor. Nonetheless, the identification of MmFAMT as a structural homolog of the SABATH class of methyltransferases extends the function of Pfam03492 (D'Auria et al., 2003) to beyond plant metabolism.

Prior studies on the plant SABATH members suggest that these enzymes do not require a general base to deprotonate the substrate methyl acceptor, as its carboxylate is likely ionized at physiological pH due to its low pK_a (Zubieta et al., 2003). Likewise, there are no residues in the active site of MmFAMT that can abstract the proton from the fatty acid carboxylate prior to methyl transfer, suggesting that the enzyme active site simply serves to facilitate proximity and orientation of the reactive groups. The side-chain amide of Gln31 and the indole nitrogen of Trp155 are within hydrogen bonding distance from the two carboxylate oxygens, and structure-guided engineering studies (Zubieta et al., 2003) demonstrate that replacement of the equivalent Gln in plant *O*-methyltransferases establishes selectivity against different methyl acceptors. The replacement of both of these residues in the MmFAMT homolog from *Mycobacterium smegmatis*

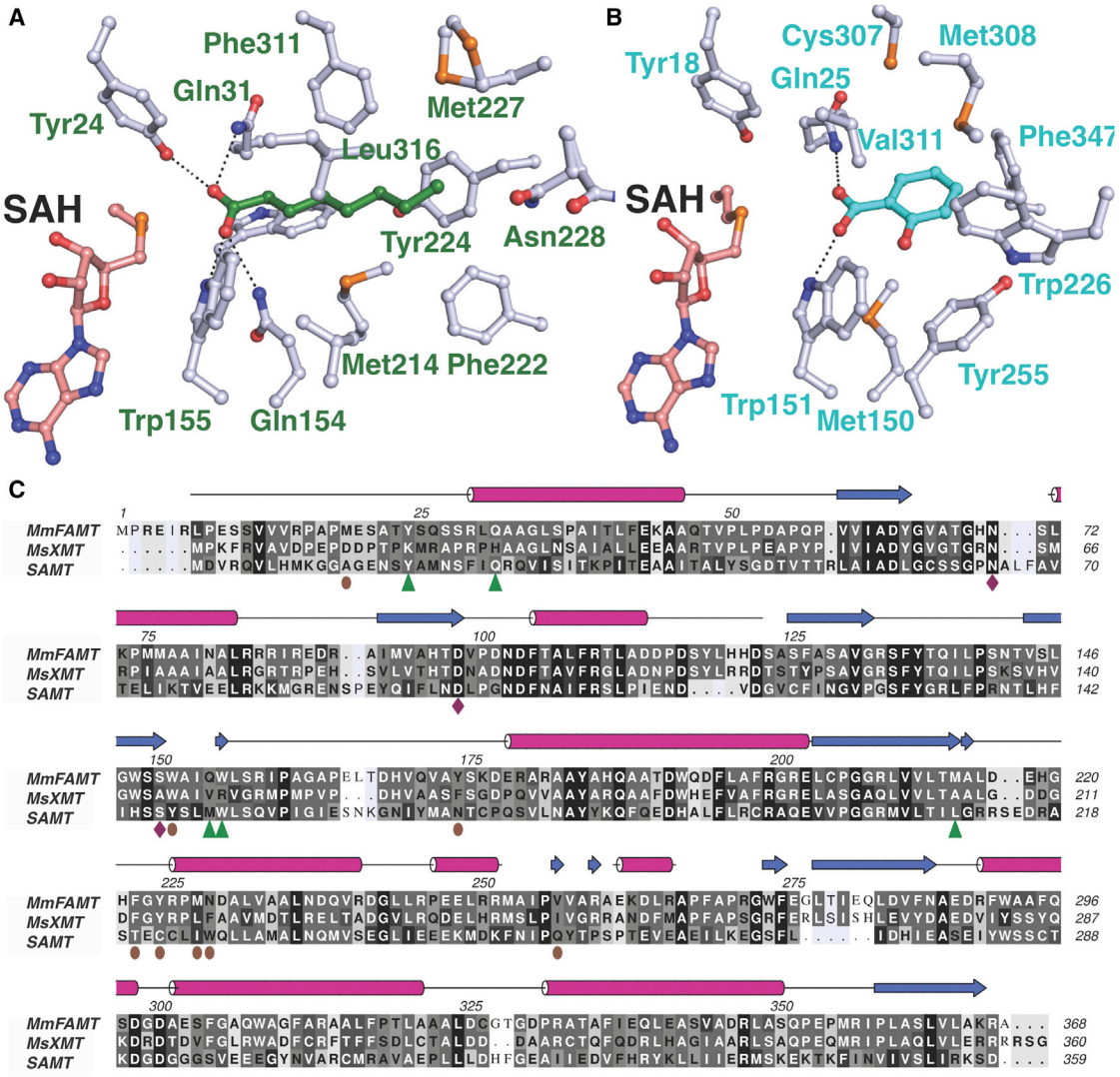

Figure 4. Methyltransferase Active Site Comparisons

(A and B) Comparison of active sites in (A) MmFAMT (gray) with bound SAH (pink), octanoic acid (green) and (B) the SABATH family enzyme SA O-methyltransferase (gray) with bound SAH (pink) and salicylic acid (cyan).

(C) Structure-based alignment of the primary sequences of MmFAMT, MsXMT, and SA *O*-methyltransferase. The green triangles demarcate residues involved in interactions with the carboxylic acid, the brown circles demarcate residues that form the fatty acid binding pocket, and the magenta diamonds indicate residues that interact with SAH/SAM.

(52% sequence identity, UniProt: A0R0D4) (MsXMT in Figure 4C) may account for the lack of activity against fatty acid substrates in the latter (Nawabi et al., 2011).

Studies of plant SABATH enzymes have determined that small changes in the primary amino acid sequence of these enzymes can establish methyltransferase activity on structural scaffolds with diverse chemical structures. Similarly, small changes in the primary sequence of mycobacterial methyltransferases homologous to MmFAMT (Figures 5 and S6) provide a pool of enzymes that have been engineered by nature to utilize fatty acids of different chain lengths. The identification of the active site residues of MmFAMT that recognize the carboxyl of the substrate as well as the residues that line the hydrophobic pocket that harbors the fatty acid tail can guide the selection of MmFAMT homologs for the in vivo production of various FAMEs of desired length.

Prior attempts to utilize MmFAMT for production of biodiesel in *E. coli* (Nawabi et al., 2011) resulted in yields that were considerably lower than for other reported fatty acid ethyl esterification processes (Steen et al., 2010). From the crystal structure of MmFAMT, as well as the previous in vivo studies (Nawabi et al., 2011), it is evident that MmFAMT can methylate medium-chain fatty acids (up to 12–14 carbons long), which could account for the low observed yields. Specifically, low compatibility between MmFAMT and the fatty acid thioesterases used to generate the fatty acid substrate would result in methylation of only a fraction of the available fatty acids. The utilization of complementary combinations of thioesterases with

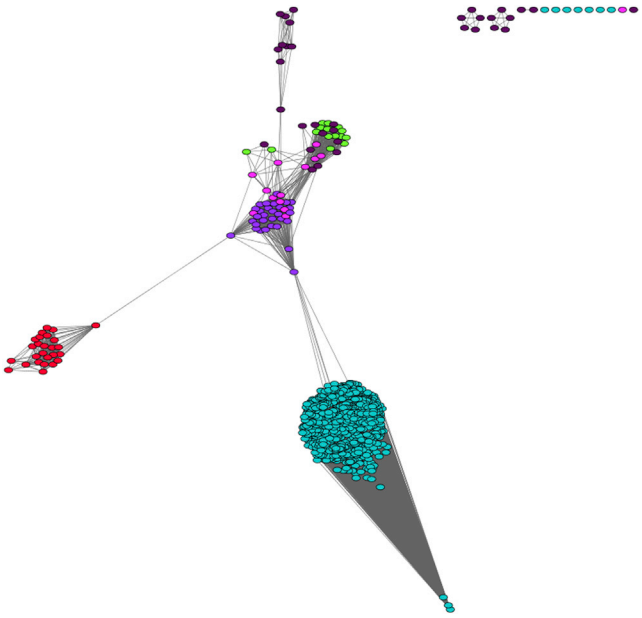

Figure 5. Sequence Similarity Network

The network (Gerlt et al., 2015; Shannon et al., 2003) contains 838 nodes and 242,549 edges. Each node represents amino acid sequences that are 95% or more identical, and each edge connects a pair of sequences at an E value of better than 1×10^{-30}. This E value is the one generated by the EFI-EST (Gerlt et al., 2015), and is not identical to E values generated by BLAST (Gerlt et al., 2015; Altschul et al., 1990; Altschul, 1993). Teal, plants; indigo, actinobacteria; fuchsia, proteobacteria; green, cyanobacteria; red, fungi; plum, other.

mycobacterial methyltransferases that accept different fatty acid substrate lengths can result in better yields. Based on our results, additional metabolic engineering, for example, overexpression of an efficient SAH nucleosidase to avert product inhibition by SAH, can further increase the methyl ester production. These data provide a starting point for engineering efforts directed at exploiting both MmFAMT and homologs for the in vivo production of various FAMEs of desired length.

SIGNIFICANCE

Methylation of free fatty acids affords a viable route toward the production of biodiesel. The structure of the mycobacterial FAMT reveals an architectural conservation with enzymes involved in plant natural product biosynthesis. Kinetic analysis of structure-based variants provides a rationale for substrate specificity. These data provide the framework for further engineering experiments aimed at expanding the substrate scope of this biotechnologically relevant catalyst.

EXPERIMENTAL PROCEDURES

Chemicals and Reagents

All chemical reagents were purchased from Sigma-Aldrich unless otherwise noted. All of the materials used for protein production and purification were purchased from GE Healthcare.

Cloning and Site-Specific Mutagenesis

MmFAMT (GenBank: NC010612; gene $MMAR_{3356}$) was amplified using PCR with template genomic DNA of *Mycobacterium marinum* strain M (ATCC BAA-535) and primers designed based on the published sequence. The gene was cloned into the NdeI/BamHI sites of a pET28b vector, and this plasmid was used as template for the generation of the site-specific mutants by PCR (Table S3). The integrity of all recombinant plasmids was confirmed by sequencing (ACGT).

Protein Expression and Purification

Expression vectors bearing wild-type or mutant MmFAMT were transformed into *E. coli* Rosetta 2(DE3) cells for heterologous protein production. A 5-ml starter culture was inoculated in 2 L of Luria-Bertani growth medium supplemented with 50 μg/ml kanamycin and 25 μg/ml chloramphenicol. The culture was grown at 37°C until the absorbance at 600 nm reached 0.6–0.8, at which point protein production was induced by addition of 0.3 mM isopropyl-β-D-1-thiogalactopyranoside. The culture was then cooled to 18°C and grown for an additional 18 hr. Cells were collected by centrifugation, resuspended in 20 mM Tris-HCl (pH 8.0), 500 mM NaCl, and 10% glycerol buffer, and lysed by multiple passages through a C5 Emulsiflex (Avestin) cell homogenizer. Following centrifugation of the lysate, the supernatant was applied to a 5-ml His-Trap (GE Biosciences) column that was previously equilibrated with 20 mM Tris-HCl (pH 8.0), 1 M NaCl, and 30 mM imidazole. The column was extensively washed with the same buffer, and elution of specifically bound protein was carried out using a gradient of increasing imidazole concentration. Fractions containing protein of the highest purity (as determined by SDS-PAGE) were pooled and the polyhistidine affinity tag was removed by overnight incubation with thrombin at 4°C. Samples were further purified using size-exclusion chromatography (Superdex HiloadTM 200 16/60) in a buffer of 20 mM HEPES (pH 7.5) and 300 mM KCl. Samples were concentrated using a 10,000-Da molecular weight cutoff Amicon centrifugal filter. SeMet MmFAMT was produced by repression of methionine biosynthesis in defined media prior to protein induction (Doublie, 1997), and was purified as described above. All proteins were flash-frozen in liquid nitrogen and stored at −80°C. Prior to freezing, 2.5% glycerol (final concentration) was added to samples of wild-type and mutant proteins used for kinetic analysis, but not to samples used for crystallographic studies.

Crystallization

Initial crystallization conditions were determined by the sparse matrix sampling method using commercial screens. Crystals of the MmFAMT/SAH complex were grown using the hanging-drop vapor diffusion method. In brief, 0.9 μl of protein at 4 mg/ml concentration was incubated with 2 mM SAM for 1 hr on ice, and was subsequently mixed with 0.9 μl of precipitant solution (0.1 M $MgCl_2$, 0.1 M *N*-(2-acetamido)iminodiacetic acid [pH 6.5], 12% polyethylene glycol 6000) and 0.2 μl of 7% (v/v) 1-butanol, and equilibrated over a well containing the same precipitant solution at room temperature. Although the crystallization media used SAM, the resultant structure revealed density corresponding to SAH, due to either hydrolysis or the presence of trace amounts of SAH in the SAM preparation. Crystals grew within 2 days, and were transiently soaked in precipitant solution supplemented with 30% glycerol prior to vitrification by direct immersion in liquid nitrogen. Ligand bound crystals were grown similarly using protein that was incubated with 2 mM SAH, 2 mM (3-hydroxy) fatty acid, and 1 mM DTT for 30 min prior to crystallization.

Data Collection, Phasing, and Structure Determination

X-Ray diffraction data were collected at Life Sciences Collaborative Access Team (LS-CAT), Sector 21, Argonne National Laboratory. All data were indexed, integrated, and scaled using either HKL2000 or XDS. Initial crystallographic phases were determined by single-wavelength anomalous diffraction from the SeMet-labeled protein crystals of the MmFAMT-SAH complex using data collected near the SE absorption edge (λ = 0.97872 Å). Due to the low symmetry of the SeMet crystals (monoclinic setting), care was taken during crystal alignment to maximize the simultaneous collection of Bijvoet pairs. A four-fold redundant dataset was collected to 1.95 Å resolution (R_{merge} of 5.5%, $I/\sigma(I)$ of 2.2 in the highest-resolution shell) using a MAR CCD detector. The heavy-atom substructure was determined using SHELX (Sheldrick, 2010). The heavy-atom positions were imported into SHARP (Bricogne et al., 2003) for maximum-likelihood refinement resulting in preliminary phases with a mean figure of merit of 0.382. Density modification using solvent flattening and non-crystallographic symmetry averaging yielded a map of exceptional

quality, which allowed for nearly all of the main chain and roughly half of the side chains to be automatically built using Buccaneer (Cowtan, 2006, 2008) as implemented in the CCP4 suite of programs (Winn et al., 2011). Additional cycles of manual rebuilding interspersed with crystallographic refinement using REFMAC5 (Murshudov et al., 2011) resulted in the final model. The final cycles of model building and refinement were carried out against high-resolution data collected on native crystals of MmFAMT-SAH.

Cocrystal structures with bound ligands were all determined by molecular replacement as implemented in the Phenix program suite (Adams et al., 2010), using the refined coordinates of SeMet MmFAMT as search model. The resultant solutions were subsequently used as starting models for several rounds of automated model building using the ARP/wARP web server (Winn et al., 2011; Murshudov et al., 2011; Langer et al., 2008), followed by rounds of manual rebuilding using Coot (Emsley et al., 2010), combined with crystallographic refinement using REFMAC5 (Murshudov et al., 2011). Ligands were built in Coot, and water molecules were added using the ARP/wARP solvent building software of the CCP4 suite (Lamzin and Wilson, 1993), and confirmed by manual inspection. In all cases, the quality of the in-progress model was routinely monitored using both the free R factor (Read et al., 2011) and MolProbity (Chen et al., 2010) for quality assurance.

Determination of Kinetic Parameters

For all experiments, SAM was further purified by high-performance liquid chromatography (HPLC) using a C18 column (Vydac; 5-μm particle size, 4.6 × 250 mm) and monitoring absorbance at 260 nm. The column was washed for 30 min with solvent B (methanol with 0.1% trifluoroacetic acid), and equilibrated for 15 min with solvent A (water with 0.1% trifluoroacetic acid). SAM was injected into the column and a gradient elution was applied as follows: wash with 5 ml of solvent A, elute with a linear gradient to a final 20% of solvent B, and wash with 5 ml of solvent B. The flow rate was 1 ml/min throughout the procedure. The fraction of SAM collected was subsequently lyophilized and stored at −20°C. Fresh solution of SAM was prepared before each experiment.

The kinetic parameters of the wild-type and mutant proteins were determined using a photospectrometric assay that monitors the production of SAH (Dorgan et al., 2006; Wooderchak et al., 2008). All enzyme reactions were performed in 100 mM HEPES (pH 7.8) and 300 mM KCl at 37°C, and monitored at 265 nm for up to 20 min. Control reactions without addition of the substrate were also included to take into account any background hydrolysis of SAM over time. For determination of the Michaelis-Menten parameters of the wild-type enzyme and mutants for the fatty acids and 3-hydroxy fatty acids, a 150-μl reaction volume contained the following components: 0.1–2.0 μM MmFAMT, 1 μM SAH nucleosidase, 0.2 μM adenine deaminase, 1 mM $MnSO_4$, 80 μM SAM, and various concentrations of fatty acids and 3-hydroxy fatty acids. For determination of the kinetic parameters for SAM, a 150-μl reaction volume contained 0.2 μM MmFAMT, 1 μM SAH nucleosidase, 0.2 μM adenine deaminase, 1 mM $MnSO_4$, 3 mM C8, and various concentrations of SAM. Based on the initial reaction rates, the apparent K_M and V_{max} values were determined using the Michaelis-Menten function of Origin (OriginLab). Results are means ± SEM of triplicate experiments.

For mutants with very increased K_M values for C8 or 3-OH-C10, saturation of the enzyme could not be achieved due to limited solubility of the substrates in the reaction buffer. In these cases, the apparent K_M and V_{max} values could not be determined, but the k_{cat}/K_M values were obtained by plotting the observed rates (k_{obs}) at four different substrate concentrations (Figure S5). For the Y24F mutant, the kinetic parameters for SAM, and consequently for C8 and 3-OH-C10, could not be determined, as the K_M value increased such that saturation of the enzyme could not be achieved due to limitations of the assay (concentration of SAM used should be kept below 250 μM to remain in the linear range of the spectrophotometer [Dorgan et al., 2006]).

To attest that the coupling enzymes were not rate limiting, the initial rates of 0.1, 0.2, and 0.4 μM wild-type enzyme were determined by addition of 3 mM C8. The means of the observed rates ± SEM were found to be the same (Figure S5A), indicating that the coupling enzymes are not rate limiting. Consequently, the measured rate corresponds to the rate of MmFAMT.

All substrates were purchased from Sigma-Aldrich, except for the 3-OH-C8, which was purchased from Matreya. The 3-hydroxy fatty acids were purchased as enantiomeric mixtures. However, it is clear from the crystal structure of the enzyme complexed with SAH and 3-OH-C10 that the enzyme utilizes only the S enantiomer (Figures 3C and S4). Subsequently, the enantiomeric ratio was determined by Mosher ester analysis (Hoye et al., 2007), and was found to be 1:1.

End-point Activity Assay

The activity of the wild-type enzyme for SA was investigated by GC-MS. 100-μl reactions containing 50 μM wild-type MmFAMT, 500 μM SAH nucleosidase, 5 mM SAM, and 10 mM substrate were incubated at 37°C for 2 hr. The samples were cleaned from the enzyme with a 10,000-Da molecular weight cutoff Amicon spin filter, and analyzed by the Roy J. Carver Biotechnology Center (University of Illinois at Urbana Champaign). All reactions were performed in the same buffer used for kinetic analysis supplemented with 5% methanol (final concentration). To confirm that methanol did not deactivate the enzyme and that possible observed inactivity was not due to its addition, reactions containing wild-type MmFAMT and C8 were included. Control reactions without addition of the enzyme were also analyzed. Results are means ± SEM of triplicate experiments.

Isothermal Titration Calorimetry

The binding affinity of wild-type MmFAMT for SAM and SAH was measured at 25°C using a VP-ITC microcalorimeter (Microcal). Protein and ligands were in the same buffer used for kinetic analysis. For binding of SAM, 1.1–1.15 mM SAM was injected into the reaction cell containing 30–35 μM protein in 28 successive aliquots at 300-s intervals and 20.5-s duration, with a reference power of 2 μcal/s. For binding of SAH, 0.52–0.54 mM SAH was injected into the reaction cell containing 40–42 μM protein in 28 successive aliquots at 240-s intervals and 20.5-s duration, with a reference power of 6 μcal/s. All injections were 10 μl in volume, except for the first injection which was 4 μl and was excluded from data analysis. The protein-ligand buffer was used in the reference cell, and a titration of the ligand into just the buffer was subtracted from the measurements. Non-linear regression with a single-site fitting model (MicroCal Origin) was applied for data analysis, and the thermodynamic parameters were calculated using the Gibbs free energy equation ($\Delta G = \Delta H - T\Delta S$) and the relationship $\Delta G = -RT\ln K_a$. Results are means ± SEM of duplicate experiments. For all binding experiments, freshly purified protein was used, and commercial preparations of SAM were purified by HPLC as described above.

Sequence Similarity Network

A sequence similarity network was generated by using the Enzyme Function Initiative Enzyme Similarity Tool (EFI-EST: http://efi.igb.illinois.edu/efi-est/) (Gerlt et al., 2015) with the sequence of MmFAMT as the query for a BLASTP (Altschul et al., 1990; Altschul, 1993) search of the UniProtKB database (http://www.uniprot.org/) (UniProt Consortium, 2015). Only sequences of 300–450 amino acids were included for the subsequent generation of a network with E-values equal to or lower than 1×10^{-30}. This network was visualized using Cytoscape 3.2.1 (Figure 5) (Shannon et al., 2003).

SUPPLEMENTAL INFORMATION

Supplemental Information includes Supporting Methods, six figures, and four tables and can be found with this article online at http://dx.doi.org/10.1016/j.chembiol.2015.09.011.

ACKNOWLEDGMENTS

We would like to thank the staff at Life Sciences Collaborative Access Team (LS-CAT, Argonne National Laboratory, Argonne, IL) for facilitating data collection, and Dr. Alexander Ulanov from the Metabolomics Center (Roy J. Carver Biotechnology Center, University of Illinois at Urbana-Champaign) for the GC-MS analysis. We would also like to thank Drs. Spencer Peck and Bijoy Desai for helpful discussions about the kinetic studies.

Received: May 13, 2015
Revised: September 4, 2015
Accepted: September 24, 2015
Published: October 29, 2015

REFERENCES

Adams, P.D., Afonine, P.V., Bunkoczi, G., Chen, V.B., Davis, I.W., Echols, N., Headd, J.J., Hung, L.-W., Kapral, G.J., Grosse-Kunstleve, R.W., et al. (2010). PHENIX: a comprehensive Python-based system for macromolecular structure solution. Acta Crystallogr. D Biol. Crystallogr. *66*, 213–221.

Akamatsu, Y., and Law, J.H. (1970). The enzymatic synthesis of fatty acid methyl esters by carboxyl group alkylation. J. Biol. Chem. *245*, 709–713.

Altschul, S.F. (1993). A protein alignment scoring system sensitive at all evolutionary distances. J. Mol. Evol. *36*, 290–300.

Altschul, S.F., Gish, W., Miller, W., Myers, E.W., and Lipman, D.J. (1990). Basic local alignment search tool. J. Mol. Evol. *215*, 403–410.

Alugupalli, S., Portaels, F., and Larsson, L. (1994). Systematic study of the 3-hydroxy fatty acid composition of mycobacteria. J. Bacteriol. *176*, 2962–2969.

Alugupalli, S., Lanéelle, M.A., Larsson, L., and Daffé, M. (1995). Chemical characterization of the ester-linked 3-hydroxy fatty acyl-containing lipids in *Mycobacterium tuberculosis*. J. Bacteriol. *177*, 4566–4570.

Atadashi, I.M., Aroua, M.K., and Aziz, A.A. (2010). High quality biodiesel and its diesel engine application: a review. Renew. Sustainable Energy Rev. *14*, 1999–2008.

Barry, C.E., III, Lee, R.E., Mdluli, K., Sampson, A.E., Schroeder, B.G., Slayden, R.A., and Yuan, Y. (1998). Mycolic acids: structure, biosynthesis and physiological functions. Prog. Lipid Res. *37*, 143–179.

Bernstein, F.C., Koetzle, T.F., Williams, G.J., Meyer, E.F., Jr., Brice, M.D., Rodgers, J.R., Kennard, O., Shimanouchi, T., and Tasumi, M. (1977). The Protein Data Bank: a computer-based archival file for macromolecular structures. J. Mol. Biol. *112*, 535–542.

Blumenthal, R.M., Cheng, X., and Fauman, E.B. (1999). Structure and Evolution of AdoMet-dependent Methyltransferases, First Edition (World Scientific), pp. 1–38.

Boissier, F., Bardou, F., Guillet, V., Uttenweiler-Joseph, S., Daffe, M., Quemard, A., and Mourey, L. (2006). Further insight into S-adenosylmethionine-dependent methyltransferases: structural characterization of Hma, an enzyme essential for the biosynthesis of oxygenated mycolic acids in Mycobacterium tuberculosis. J. Biol. Chem. *281*, 4434–4445.

Bricogne, G., Vonrhein, C., Flensburg, C., Schiltz, M., and Paciorek, W. (2003). Generation, representation and flow of phase information in structure determination: recent developments in and around SHARP 2.0. Acta Crystallogr. D Biol. Crystallogr. *59*, 2023–2030.

Chen, V.B., Arendall, W.B., Headd, J.J., Keedy, D.A., Immormino, R.M., Kapral, G.J., Murray, L.W., Richardson, J.S., and Richardson, D.C. (2010). MolProbity: all-atom structure validation for macromolecular crystallography. Acta Crystallogr. D Biol. Crystallogr. *66*, 12–21.

Choi-Rhee, E., and Cronan, J.E. (2005). A nucleosidase required for in vivo function of the S-adenosyl-L-methionine radical enzyme, biotin synthase. Chem. Biol. *12*, 589–593.

Cowtan, K. (2006). The Buccaneer software for automated model building. 1. Tracing protein chains. Acta Crystallogr. D Biol. Crystallogr. *62*, 1002–1011.

Cowtan, K. (2008). Fitting molecular fragments into electron density. Acta Crystallogr. D Biol. Crystallogr. *64*, 83–89.

D'Auria, J.C., Chen, F., and Pichersky, E. (2003). The SABATH family of MTS in Arabidopsis thaliana and other plant species. In Recent Advances in Phytochemistry, T.R. John, ed. (Elsevier), pp. 253–283.

Demirbaş, A. (2002). Diesel fuel from vegetable oil via transesterification and soap pyrolysis. Energy Sourc. *24*, 835–841.

Dorgan, K.M., Wooderchak, W.L., Wynn, D.P., Karschner, E.L., Alfaro, J.F., Cui, Y., Zhou, Z.S., and Hevel, J.M. (2006). An enzyme-coupled continuous spectrophotometric assay for S-adenosylmethionine-dependent methyltransferases. Anal. Biochem. *350*, 249–255.

Doublie, S. (1997). Preparation of selenomethionyl proteins for phase determination. Methods Enzymol. *276*, 523–530.

Emsley, P., Lohkamp, B., Scott, W.G., and Cowtan, K. (2010). Features and development of Coot. Acta Crystallogr. D Biol. Crystallogr. *66*, 486–501.

Gerlt, J.A., Bouvier, J.T., Davidson, D.B., Imker, H.J., Sadkhin, B., Slater, D.R., and Whalen, K.L. (2015). Enzyme Function Initiative-Enzyme Similarity Tool (EFI-EST): a web tool for generating protein sequence similarity networks. Biochim. Biophys. Acta *1854*, 1019–1037.

Glickman, M.S. (2003). The mmaA2 gene of *Mycobacterium tuberculosis* encodes the distal cyclopropane synthase of the alpha-mycolic acid. J. Biol. Chem. *278*, 7844–7849.

Glickman, M.S., Cox, J.S., and Jacobs, W.R., Jr. (2000). A novel mycolic acid cyclopropane synthetase is required for cording, persistence, and virulence of *Mycobacterium tuberculosis*. Mol. Cell *5*, 717–727.

Holm, L., and Rosenstrom, P. (2010). Dali server: conservation mapping in 3D. Nucleic Acids Res. *38*, W545–W549.

Hoye, T.R., Jeffrey, C.S., and Shao, F. (2007). Mosher ester analysis for the determination of absolute configuration of stereogenic (chiral) carbinol carbons. Nat. Protoc. *2*, 2451–2458.

Huang, C.C., Smith, C.V., Glickman, M.S., Jacobs, W.R., Jr., and Sacchettini, J.C. (2002). Crystal structures of mycolic acid cyclopropane synthases from *Mycobacterium tuberculosis*. J. Biol. Chem. *277*, 11559–11569.

Kung, Y., Runguphan, W., and Keasling, J.D. (2012). From fields to fuels: recent advances in the microbial production of biofuels. ACS Synth. Biol. *1*, 498–513.

Kung, P.-P., Huang, B., Zehnder, L., Tatlock, J., Bingham, P., Krivacic, C., Gajiwala, K., Diehl, W., Yu, X., and Maegley, K.A. (2015). SAH derived potent and selective EZH2 inhibitors. Bioorg. Med. Chem. Lett. *25*, 1532–1537.

Lamzin, V.S., and Wilson, K.S. (1993). Automated refinement of protein models. Acta Crystallogr. D Biol. Crystallogr. *49*, 129–147.

Langer, G., Cohen, S.X., Lamzin, V.S., and Perrakis, A. (2008). Automated macromolecular model building for X-ray crystallography using ARP/wARP version 7. Nat. Protoc. *3*, 1171–1179.

Lee, W.J., Shim, J.Y., and Zhu, B.T. (2005). Mechanisms for the inhibition of DNA methyltransferases by tea catechins and bioflavonoids. Mol. Pharmacol. *68*, 1018–1030.

Leung, D.Y.C., Wu, X., and Leung, M.K.H. (2010). A review on biodiesel production using catalyzed transesterification. Appl. Energy *87*, 1083–1095.

Li, Q., Du, W., and Liu, D. (2008). Perspectives of microbial oils for biodiesel production. Appl. Microbiol. Biotechnol. *80*, 749–756.

Liscombe, D.K., Louie, G.V., and Noel, J.P. (2012). Architectures, mechanisms and molecular evolution of natural product methyltransferases. Nat. Prod. Rep. *29*, 1238–1250.

Marrakchi, H., Lanéelle, M.-A., and Daffé, M. (2014). Mycolic acids: structures, biosynthesis, and beyond. Chem. Biol. *21*, 67–85.

McCarthy, A.A., and McCarthy, J.G. (2007). The structure of two N-methyltransferases from the caffeine biosynthetic pathway. Plant Physiol. *144*, 879–889.

Murshudov, G.N., Skubak, P., Lebedev, A.A., Pannu, N.S., Steiner, R.A., Nicholls, R.A., Winn, M.D., Long, F., and Vagin, A.A. (2011). REFMAC5 for the refinement of macromolecular crystal structures. Acta Crystallogr. D Biol. Crystallogr. *67*, 355–367.

Naik, S.N., Goud, V.V., Rout, P.K., and Dalai, A.K. (2010). Production of first and second generation biofuels: a comprehensive review. Renew. Sustainable Energy Rev. *14*, 578–597.

Nawabi, P., Bauer, S., Kyrpides, N., and Lykidis, A. (2011). Engineering *Escherichia coli* for biodiesel production utilizing a bacterial fatty acid methyltransferase. Appl. Environ. Microbiol. *77*, 8052–8061.

Obianyo, O., and Thompson, P.R. (2012). Kinetic mechanism of protein arginine methyltransferase 6 (PRMT6). J. Biol. Chem. *287*, 6062–6071.

Orpiszewski, J., Hebda, C., Szykuła, J., Powls, R., Clasper, S., and Rees, H.H. (1991). Multiple forms of O-methyltransferase involved in the microbial conversion of abietic acid into methyl abietate by *Mycobacterium* sp. FEMS Microbiol. Lett. *82*, 233–236.

Read, R.J., Adams, P.D., Arendall, W.B., 3rd, Brunger, A.T., Emsley, P., Joosten, R.P., Kleywegt, G.J., Krissinel, E.B., Lutteke, T., Otwinowski, Z.,

et al. (2011). A new generation of crystallographic validation tools for the protein data bank. Structure *19*, 1395–1412.

Sacco, E., Covarrubias, A.S., O'Hare, H.M., Carroll, P., Eynard, N., Jones, T.A., Parish, T., Daffe, M., Backbro, K., and Quemard, A. (2007). The missing piece of the type II fatty acid synthase system from *Mycobacterium tuberculosis*. Proc. Natl. Acad. Sci. USA *104*, 14628–14633.

Safayhi, H., Anazodo, M.I., and Ammon, H.P. (1991). Calmodulin- and Ca2(+)-insensitive fatty acid methyltransferase from RINm5F cells. Inhibition by trifluoperazine and W7. Int. J. Biochem. *23*, 769–772.

Sastry, B.V., Vidaver, P.S., Janson, V.E., and Franks, J.J. (1994). S-adenosyl-L-methionine-mediated enzymatic methylations in the rat retinal membranes. J. Ocul. Pharmacol. *10*, 253–263.

Shannon, P., Markiel, A., Ozier, O., Baliga, N.S., Wang, J.T., Ramage, D., Amin, N., Schwikowski, B., and Ideker, T. (2003). Cytoscape: a software environment for integrated models of biomolecular interaction networks. Genome Res. *13*, 2498–2504.

Sheldrick, G. (2010). Experimental phasing with SHELXC/D/E: combining chain tracing with density modification. Acta Crystallogr. D Biol. Crystallogr. *66*, 479–485.

Shimakata, T., Fujita, Y., and Kusaka, T. (1979). Purification and characterization of 3-hydroxyacyl-CoA dehydrogenase of *Mycobacterium smegmatis*. J. Biochem. *86*, 1191–1198.

Steen, E.J., Kang, Y., Bokinsky, G., Hu, Z., Schirmer, A., McClure, A., Del Cardayre, S.B., and Keasling, J.D. (2010). Microbial production of fatty-acid-derived fuels and chemicals from plant biomass. Nature *463*, 559–562.

Struck, A.W., Thompson, M.L., Wong, L.S., and Micklefield, J. (2012). S-adenosyl-methionine-dependent methyltransferases: highly versatile enzymes in biocatalysis, biosynthesis and other biotechnological applications. Chembiochem *13*, 2642–2655.

UniProt Consortium. (2015). UniProt: a hub for protein information. Nucleic Acids Res. *43*, D204–D212.

US Government. (2007). Energy Independence and Security Act of 2007 (EISA). Public Law *110-140*, 1492–1801.

Williams, K.J., Boshoff, H.I., Krishnan, N., Gonzales, J., Schnappinger, D., and Robertson, B.D. (2011). The *Mycobacterium tuberculosis* β-oxidation genes echA5 and fadB3 are dispensable for growth in vitro and in vivo. Tuberculosis (Edinb.) *91*, 549–555.

Winn, M.D., Ballard, C.C., Cowtan, K.D., Dodson, E.J., Emsley, P., Evans, P.R., Keegan, R.M., Krissinel, E.B., Leslie, A.G., McCoy, A., et al. (2011). Overview of the CCP4 suite and current developments. Acta Crystallogr. D Biol. Crystallogr. *67*, 235–242.

Wooderchak, W.L., Zhou, Z.S., and Hevel, J. (2008). Assays for S-adenosyl-methionine (AdoMet/SAM)-dependent methyltransferases. Curr. Protoc. Toxicol., Chapter 4, Unit4.26.

Yuan, Y., and Barry, C.E. (1996). A common mechanism for the biosynthesis of methoxy and cyclopropyl mycolic acids in *Mycobacterium tuberculosis*. Proc. Natl. Acad. Sci. USA *93*, 12828–12833.

Yuan, Y., Lee, R.E., Besra, G.S., Belisle, J.T., and Barry, C.E., 3rd (1995). Identification of a gene involved in the biosynthesis of cyclopropanated mycolic acids in *Mycobacterium tuberculosis*. Proc. Natl. Acad. Sci. USA *92*, 6630–6634.

Yuan, Y., Zhu, Y., Crane, D.D., and Barry, C.E., 3rd (1998). The effect of oxygenated mycolic acid composition on cell wall function and macrophage growth in *Mycobacterium tuberculosis*. Mol. Microbiol. *29*, 1449–1458.

Zhao, N., Ferrer, J.L., Ross, J., Guan, J., Yang, Y., Pichersky, E., Noel, J.P., and Chen, F. (2008). Structural, biochemical, and phylogenetic analyses suggest that indole-3-acetic acid methyltransferase is an evolutionarily ancient member of the SABATH family. Plant Physiol. *146*, 455–467.

Zubieta, C., He, X.Z., Dixon, R.A., and Noel, J.P. (2001). Structures of two natural product methyltransferases reveal the basis for substrate specificity in plant O-methyltransferases. Nat. Struct. Biol. *8*, 271–279.

Zubieta, C., Kota, P., Ferrer, J.L., Dixon, R.A., and Noel, J.P. (2002). Structural basis for the modulation of lignin monomer methylation by caffeic acid/5-hydroxyferulic acid 3/5-O-methyltransferase. Plant Cell *14*, 1265–1277.

Zubieta, C., Ross, J.R., Koscheski, P., Yang, Y., Pichersky, E., and Noel, J.P. (2003). Structural basis for substrate recognition in the salicylic acid carboxyl methyltransferase family. Plant Cell *15*, 1704–1716.